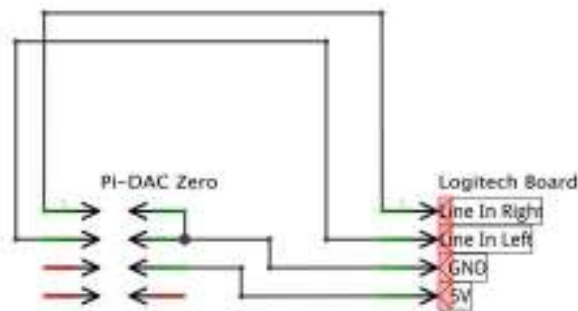


**Figure 37: 3D model of Raspberry Pi + Pi-DAC Zero holder for mounting inside Z150 speaker**

The Logitech amplifier board is connected to the Pi-DAC Zero via the 2x4 header on the Pi-DAC Zero, which provides line-out left/right, as well as GND and a 5V power supply (see Figure 38 for details of the wiring). Note that the original power supply connection is unmounted from the speaker system.



**Figure 38: Wiring of the Pi-DAC 2x4 header to the Logitech board inside the speaker**

As an alternative to building the sound module hardware into the Z150 speakers, a separate housing has been designed, in case the Raspberry Pi and Pi-DAC Zero should be connected to an existing sound system or alternative speakers. Figure 39 shows the 3D model of the case divided into two parts.

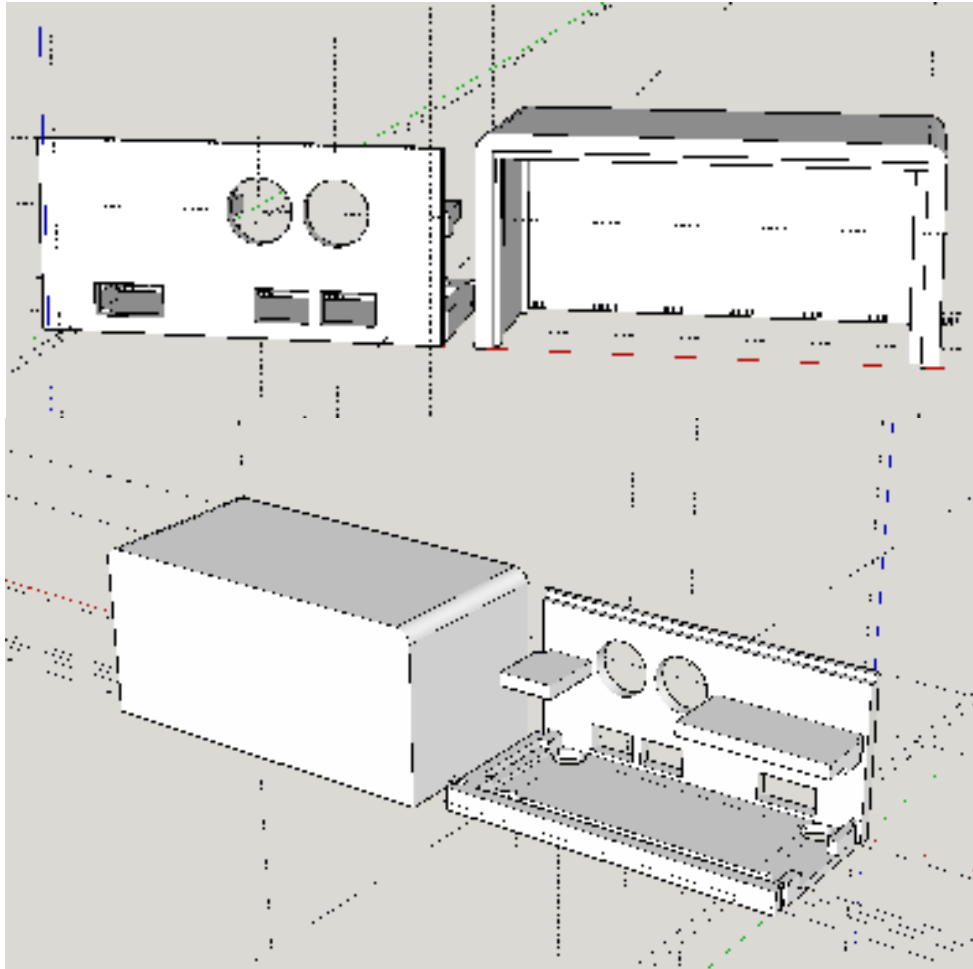


**Figure 39: 3D model of separate housing for sound module logics**

During the field test, the Logitech speakers with the built-in sound module have been used (see Table 3 for a list of required components).

**Table 3: GREAT Sound Module hardware component list**

1	Raspberry Pi Zero W board
1	IQaudio PiZero DAC
1	Micro USB Power Supply, 1A
1	microSDHC card, 16GB, Class 10 (industrial)
1	Logitech Z150 Speaker Pair

The external sound module has been used in combination with a high-quality active speaker (Pioneer RM05) for testing inside the GREAT cabin. This speaker has an advertised

frequency range of 40-50.000 Hz, and therefore a significantly better reproduction of ultrasonic sound range.



**Figure 40: External sound module with a Pioneer RM05 Speaker featuring a frequency range of 40-50.000Hz**

### 3.3 Speaker Covers

To prevent accidental adjustment of the speaker volume by the built-in volume adjustment knobs, a selection of speaker covers has been designed. For the field tests, the minimalist grey cover has been preferred (see Figure 41).

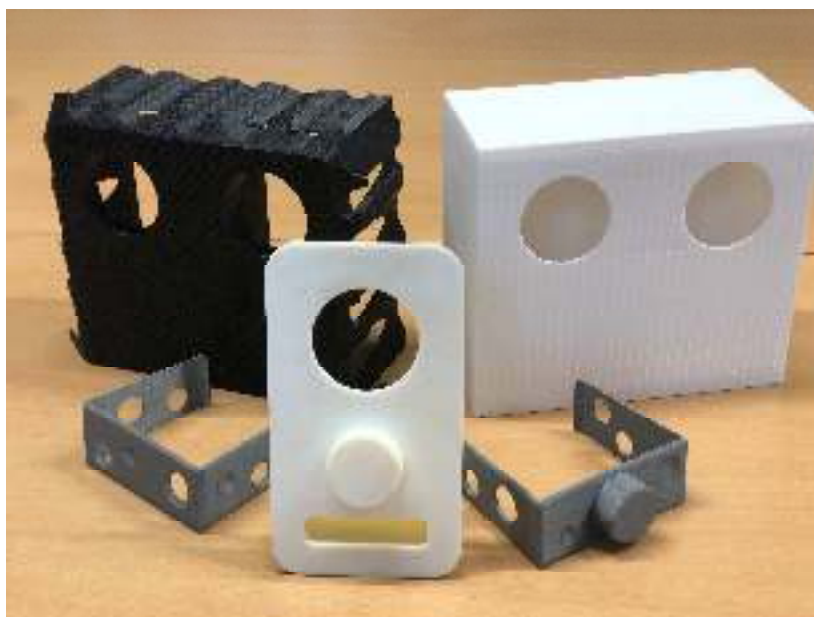


**Figure 41: Speaker covers to prevent accidental adjustment of volume level**

## 4 Scent Module

Compared to the field trial phase the scent module was reworked significantly: the casing presented in D2.1 as an outlook was further adapted, one-part 3D-printed and the other vacuum-formed. The pumping mechanism was changed from piston-based to spring-loaded. Further smaller changes will be presented in the sub-chapters below.

### 4.1 Basic Considerations

The GREAT-system requires a scent-module, which can adequately enhance the room atmosphere by dispersing respective odors. This basic requirement has not changed since the beginning of the project and we continue using spray-based dispersion for our field-test phase. Due to feedback from the tests so far hardware upgrades on the in- and outside of the device were necessary. The scent module should look more appealing and be able to resist harsher external influences (the previously used acrylic glass could shatter and did not look professional enough).

As stated further below, the pump mechanism from the functional test phase was not satisfying (a small portion of the droplets were too big and left stains on surrounding furniture), therefore the activation mechanism of the scent module was also improved. Changing the method of dispersion completely was considered (to either ultrasonic or heat vaporization), but next to the downsides already mentioned in D2.1 – involuntary vaporization, ultrasonic noise (which conflicts with the sound module) and alteration of the scent molecules (due to heat) – financially it was not an option to develop a completely new scent module.

### 4.2 Mechanical Design

Feedback during the early field-test-phase stated that the piston-based pumping mechanism created droplets of an undesirable size (too big). These droplets did not vaporize on their way from the bottle to the ground but left visible drops on the furniture or floor below. After the final vaporization there, a dry stain could still be seen.

We identified the sinusoidal stroke of the piston as the main problem: for a pump-action-based disperser, the last part of the compression is the most significant one, as the pump-head is fully loaded with liquid and when pressed appropriately quickly, it will create the desired scent-cloud. Unfortunately, the sinusoidal stroke does not allow for this, as the speed of the piston decelerates. Figure 42 shows a sinusoidal stroke, data used for linearization and a linear approximation, which would continue with constant speed until the maximum stroke.

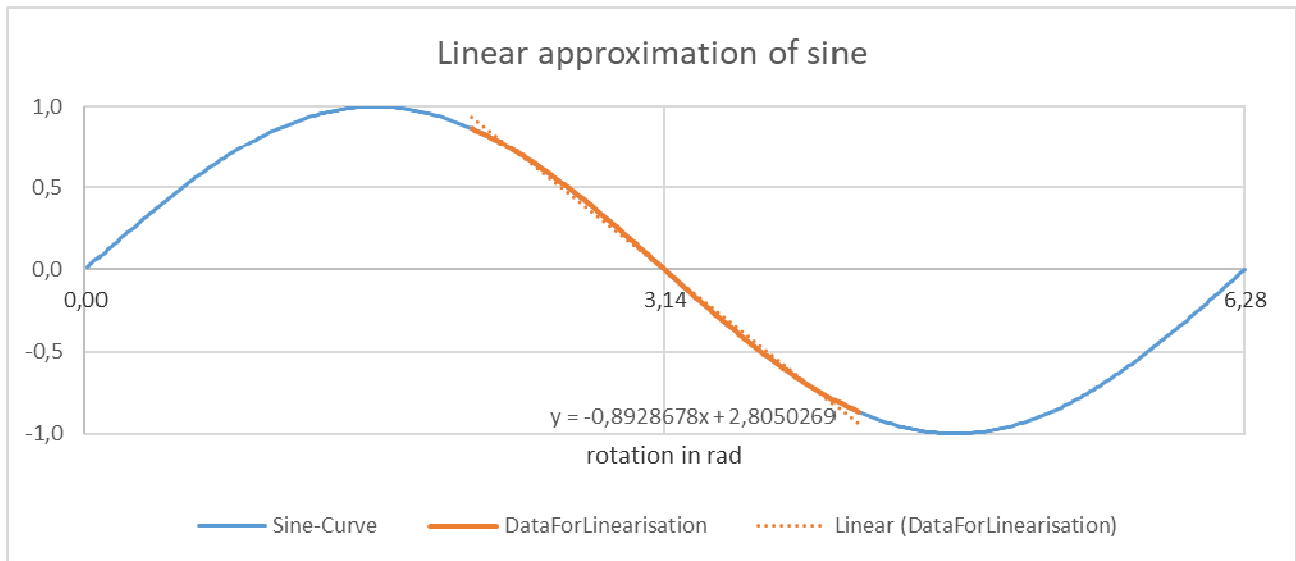


**Figure 42: Sine, linearization and database for linearization and formula for the linear approximation**

The error between that approximation and the sine curve can be seen in Figure 43. After 226 degrees, the sine starts to decelerate more and more, which means that during the last quarter of a stroke, the scent module would dispense at decreasing velocity, which lead to the undesired droplet size. In figures x and y, a stroke starts at 90 degrees and ends at 270 degrees. This means, one stroke lasts for 180 degrees (half of a rotation). The difference between 226 and 270 is 44, which makes up a quarter of one stroke.

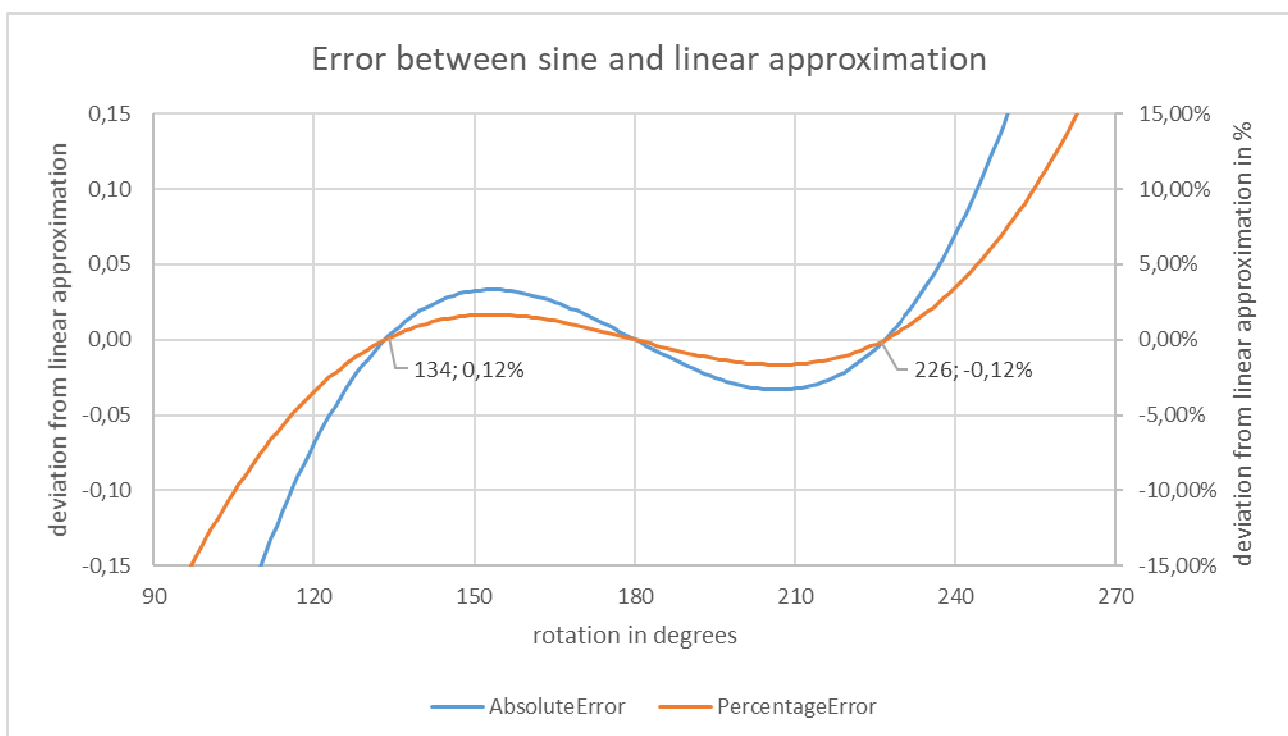


**Figure 43: Error between sine and linear approximation, absolute [-1, 1] and percentage**

To avoid this problem, we remodeled the interior parts of the casing, with the major change being the removal of the piston and the addition of a spring as seen in Figure 44. The moving parts of the mechanism were previously milled at the FH Vorarlberg. During the redesign, an iterative design process was used, where each step of the evolution was 3D-printed. Figure 44 shows the four new parts responsible for releasing the scent. The part seen on top fixes the motor, prevents the gears from slipping away, attaches to one end of the spring and the lever. As it is the only non-moving part, it will be referenced as “mount”. The redesigned piston (as seen in the left half of the center row in Figure 44) now is disconnected from the other parts and only attaches to the linear guide. The final iterations also contain a screw to stop the piston from falling off the linear guide when changing the bottles. The eccentric (as seen in the right half of the center row in Figure 44) is held in place within a gear by a perpendicular screw and catches the lever on each rotation. The lever (as seen in the bottom row of in Figure 44) is attached to the mount at two points: a screw at the bottom, allowing it to pivot and with the spring at the top.



**Figure 44: Evolution of mount (top), piston (center left), eccentric (center right) and lever (bottom)**

The motor and the gears remain, but now they spin an eccentric which in the one half of a rotation simultaneously stretches a spring and moves the lever away from the bottle, allowing the pump head to rise to its normal level (seen on the right side of Figure 45). At the maximum stroke, it moves away from the lever, which is then pulled onto the piston by the spring, which leads the force to the pump head (seen on the left side of Figure 45). The motor then continues to spin without load until the eccentric catches the lever again.

Figure 46 shows the mechanic as installed in the field-test prototypes. It was replaced in all field-test-modules between March and May 2019. For a video of the new functionality, please visit our twitter page: [https://twitter.com/GREAT\\_AAL/status/1111238884720033792](https://twitter.com/GREAT_AAL/status/1111238884720033792).

The total amount of parts required was reduced and assembling the module is now faster than before. Replacement parts can be printed at the FH Vorarlberg should any damages occur. Using our own 3D-printers instead of purchased parts presents a valuable reduction in costs for our field test prototypes.

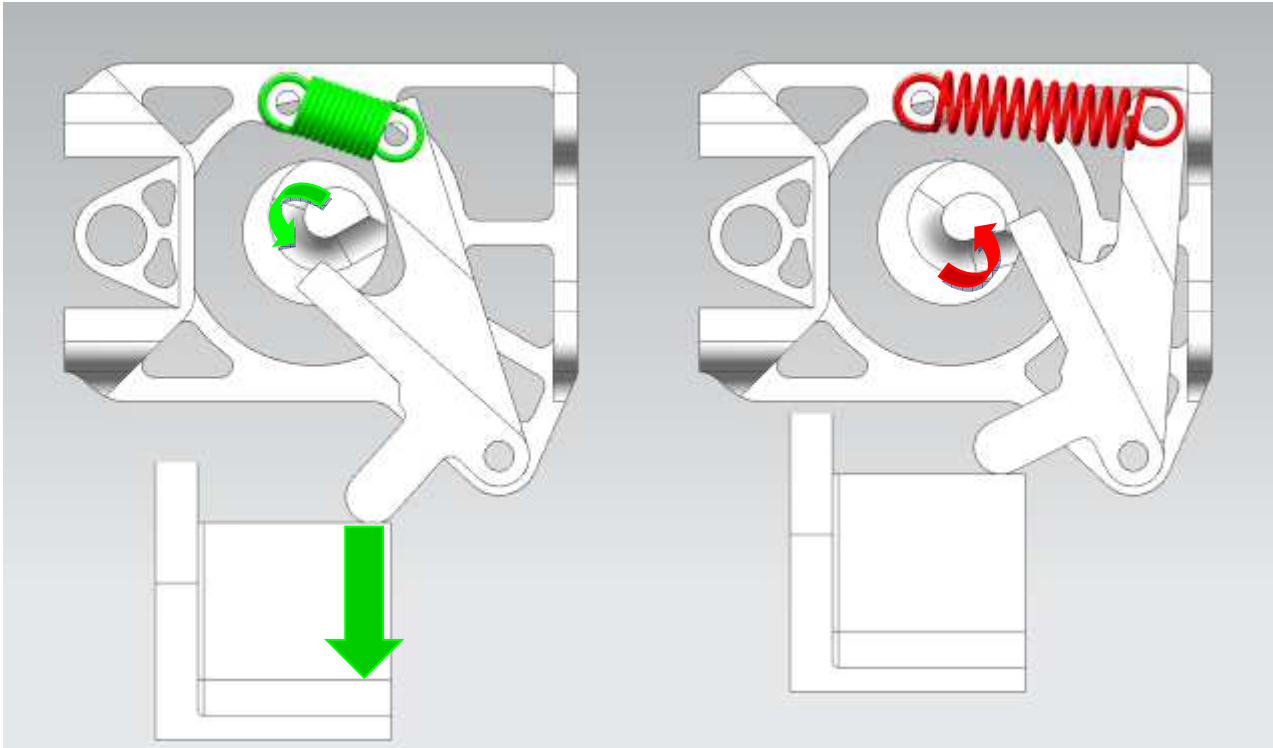


**Figure 45: Left shows the no-load-phase of the motor, right shows the spring-tensioning-phase of the motor**

For the new mechanism we need two additional screws (the ones preventing the piston from sliding off the linear guide) but less nuts as all but two screws (they can be seen in Figure 46 on the right, being screwed from the outside into the mount) directly screw into the 3D-printed material.



**Figure 46: Reworked mechanic installed in the rear casing**

### 4.3 Casing

The casing consists of two main parts: a front part (evolution as seen in Figure 47), a rear part, and a small inner casing to protect the microcontroller. In 2018 we also used optional shields (also seen in Figure 47) to prevent bigger droplets from hitting furniture. However, these shields have been retired, as the reworked mechanism vaporizes the scent liquid sufficiently.



**Figure 47: Evolution of the 3D-printed front casing (top) and the two variants of shields (bottom)**

#### 4.3.1 Front Casing

To create an appealing look, which visually connects light, and scent module, the previous casing (left casing in Figure 47) was reworked with an external designer (center casing in Figure 47) who also helped creating the cooling body for the lamp. The final design (right casing in Figure 47) has rounded edges and (not visible in this picture) increased space for the motors inside.

The production of the resulting 3D-model was outsourced to a local company, specializing in small series production. The actual manufacturing-process is vacuum forming, as it creates a nice-looking finish and has appropriate mechanical durability.

When the Raspberry Pi is connected to its power source, the front casing cannot be removed, as the plug locks it in place. This was introduced to prevent modules from spraying at users servicing them. The front casing can also be seen in Figure 48 on the right side.





**Figure 48: Left shows the completely mounted rear casing, right shows the front casing**

#### 4.3.2 Rear Casing

As before, the rear casing holds all mechanical and electrical parts as well as the bottled scents (see Figure 48, left side). Previously, it consisted of two identical aluminium bodies and a separate plate, where the microcontroller could be mounted.

During the redesign, all parts were fused together and then were 3D-printed at the local company, which vacuum-formed the front casing. Apart from mounting-holes for the screws, which were adopted from the aluminium cases, cable guides, pockets for the VOC-sensor and a possible sound level meter (not integrated) and louvers were implemented.

#### 4.3.3 Raspberry Pi Casing

We also decided to encase the microcontroller (see chapter 4.4) for the scent module in a 3D-printed box (see Figure 49). The three reasons for this were:

- Protection (ESD problematic or purely mechanical damages)
- Preventing mishandling the 2<sup>nd</sup> USB-connector
- Easier fitting to the rear casing: instead of 4 screws, 4 nuts, 4 plastic spacers and 12 isolation rings, only the Raspberry Pi casing, 2 screws and 2 nuts are required. Mounting all pieces is now much easier, as no parts can come loose at any time (the isolation rings and spacers tended to slip away when a screw was removed).

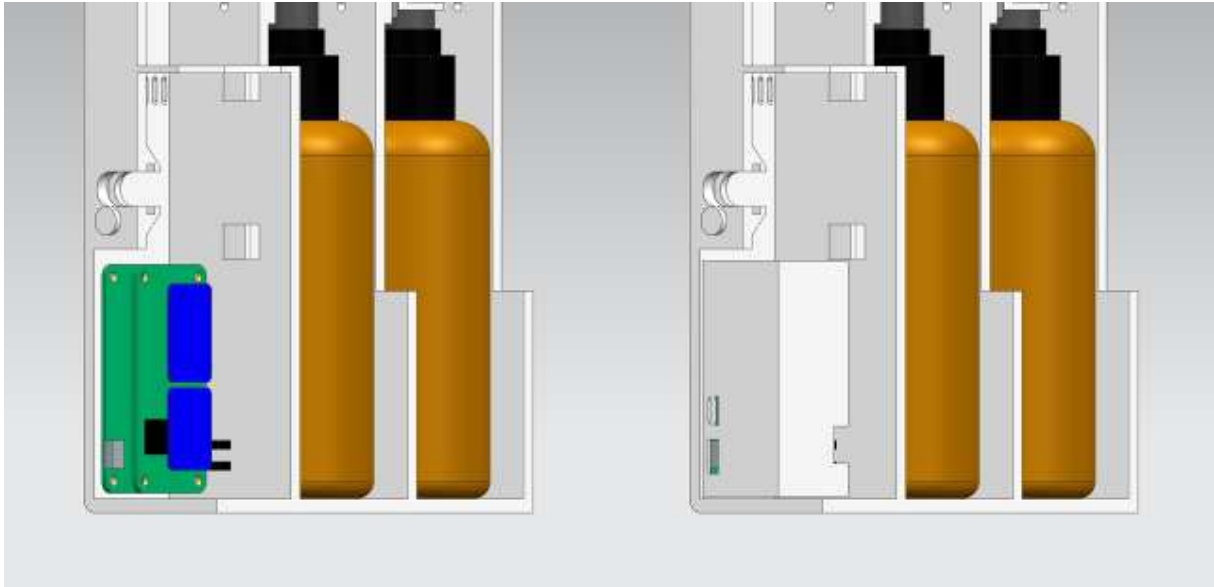


**Figure 49: Microcontroller; left unprotected; right covered**

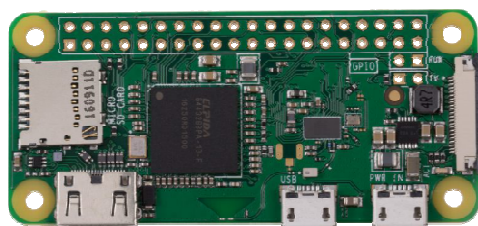
#### 4.3.4 Droplet shield

Before reworking the piston-mechanism, we reduced the amount of visible droplets by creating removable shields. They were clipped onto the front casing and prevented droplets from leaving the scent module and therefore also from creating stains on furniture. The first design (reminiscent of a smiley-face) successfully caught most of the droplets in a small integrated basin but was too airtight for adequate vaporization of the scents.

The second design (which included bigger holes, projected from the front casing) was designed to allow improved airflow past the caught scent, but the vaporization still was not enough. The shields can be seen in Figure 47.

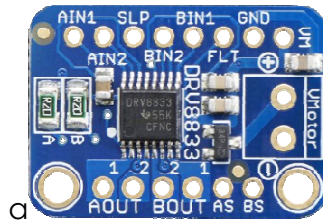
## 4.4 Electrical Design

The scent module is powered by a USB power supply rated at 5V/1A. The main electrical components of the scent module are a controller board, a motor driver unit for the motors and an analog digital converter (ADC) for system feedback. The actuators of the scent module are controlled by a Raspberry Pi Zero W board (see Figure 50), that allows for connection to a building automation system over WLAN and handles the logics of dispensing.



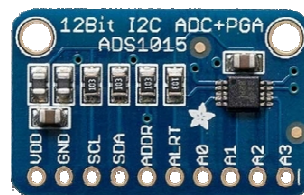
**Figure 50: Raspberry Pi Zero W board computer**

The motors of the scent module are connected to the Raspberry Pi Zero board via an Adafruit DRV8833 motor driver board that features current limiting (both, for protecting the power supply against overload in case the motor is locked, and against injuries) as well as reverse voltage protection for the controller board. One DRV8833 board allows for the connection of up to two motors (see Figure 51). The DRV8833 board is controlled over digital outputs of the GPIO header of the Raspberry board and provides fault input via a digital input.



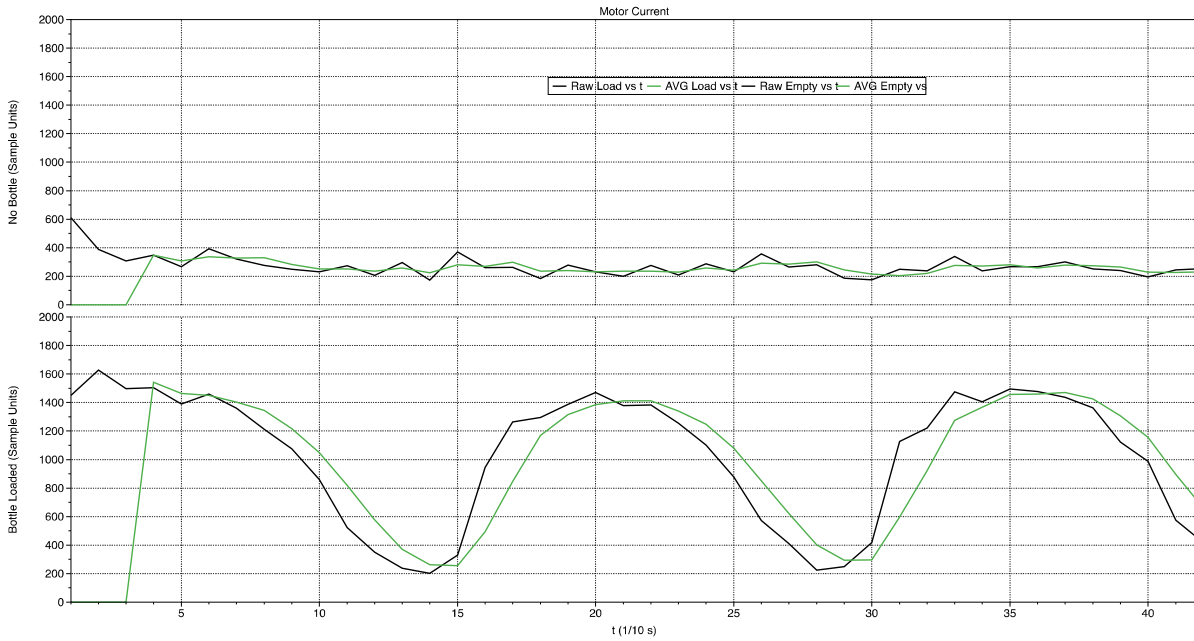
**Figure 51: Adafruit DRV8833 motor driver breakout board.**

An Adafruit ADS1015 ADC module (featuring 12-bit resolution) is used to measure the current flowing to the motors via a shunt resistor (see Figure 52). The ADC module is connected via an I2C interface to the main controller board.



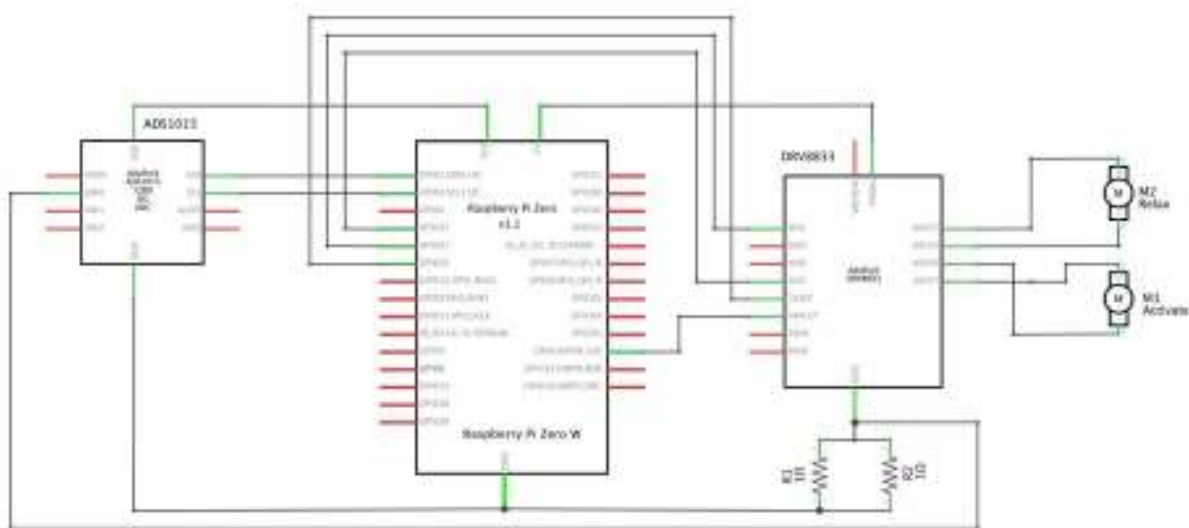
**Figure 52: Adafruit 12bit ADC converter ADS1015 breakout board**

By measuring the current flowing to the motors, the software can detect peaks and values, which relate to the inverse current position of the pump spray. This allows for automatic turn off at the upper position, which allows for easy removal and insertion of scent bottles. Also, the exact number of actuations of the pump spray can be detected in this way (see Figure 53 for typical current flow of the prototype loaded with bottles and without bottles).



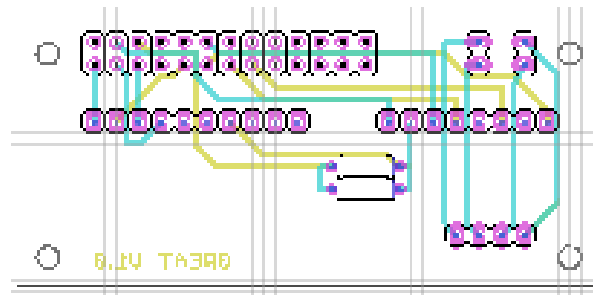
**Figure 53: Current flow to motor during pump cycles with no bottle inserted (top), and bottle inserted bottom) as raw signal and smoothed signal.**

Figure 54 shows the detailed wiring of the DRV8833 and ADS1015 modules to the Raspberry board.



**Figure 54: Schematics for the electrical components of the scent module.**

While the first prototypes built for functional testing were wired manually, a printed circuit board (PCB) has been designed to make the assembly easier for the field test prototypes. Figure 55 shows the circuit board layout, providing headers to directly plug the individual boards together.



**Figure 55: Printed circuit board design for the scent module electronics.**

#### 4.4.1 Environmental sensor

For the final field test design, we decided to put an environmental sensor into each scent module, since it became clear, that variations in test settings required continuous monitoring of air quality. The respective data is used to measure the effect dispensing scent and to prevent oversaturation.

The environmental sensor module is mounted on the left top corner of the scent module housing, pointing to the side, as seen in Figure 56 and in Figure 49. This position was chosen, to prevent actual droplets from hitting the sensor and actually measure the contents of the air without direct exposure to the spray channel.

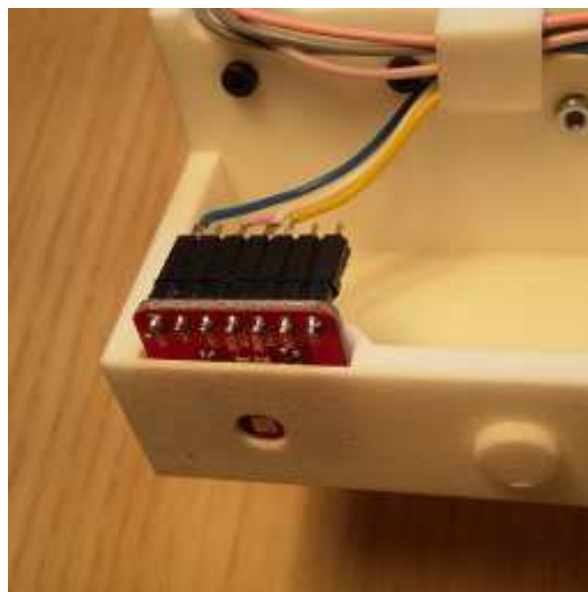


**Figure 56: VOC sensor mounting**

Table 4 shows the hardware component list for the electrical parts of the scent module.

**Table 4: GREAT Scent Module hardware component list**

1	Raspberry Pi Zero W board
1	Adafruit DRV8833 motor driver breakout board
1	Adafruit ADS1015 ADC breakout board
1	Micro USB Power Supply, 1A
1	microSDHC card, 16GB, Class 10 (industrial)
2	Resistors 1Ohm ¼ Watt
2	Pololu Micro Metal Gear Motor 6V 30:1
1	Watterott Bosch BME680 breakout board

#### 4.5 Functional Tests

Concerning electronics, the functional and field tests were successful for the scent module, no malfunctions, errors or weaknesses occurred.

## 5 Repeater

During adaptations to the field test setups at the testing places in Hall and Neumarkt, reception issues of EnOcean telegrams between the controller and the luminaires have been discovered. Due to the metal casing of the luminaire, and the unavoidable electromagnetic noise produced by LED drivers, the EnOcean performance is significantly reduced compared to e.g. PIR sensors which only have a plastic housing.

To work around this limited range of EnOcean telegrams, a special purpose repeater was developed, that besides the standard EnOcean repeating functionality also offered a logging functionality of received telegrams and their signal strength, to assist in finding the best placements of the repeaters and reconstruct what was going on, if a luminaire did not handle a switching command.

The GREAT Repeater is based on a Raspberry Pi Zero with an EnOcean TCM310 transceiver module (see Figure 57). The transceiver board is directly attached to the GPIO Header of the Raspberry Pi Zero. The transceiver module can be configured to run as a level 1 (only one step forwarding) or a level 2 (multistep forwarding) repeater and also allows for setting filters (e.g. depending on the signal level) for which telegrams should be repeated. This way EnOcean traffic caused by repeating signals can be reduced to a minimum. The Raspberry Pi and the EnOcean module are placed inside a 3D printed housing (see Figure 58).

The software running on the Raspberry Pi reads received telegrams from the transceiver module over the UART port and forwards them via a WLAN connection to a configurable receiver.

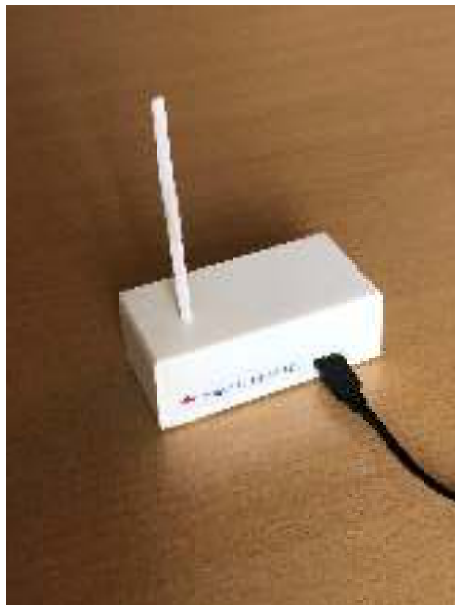
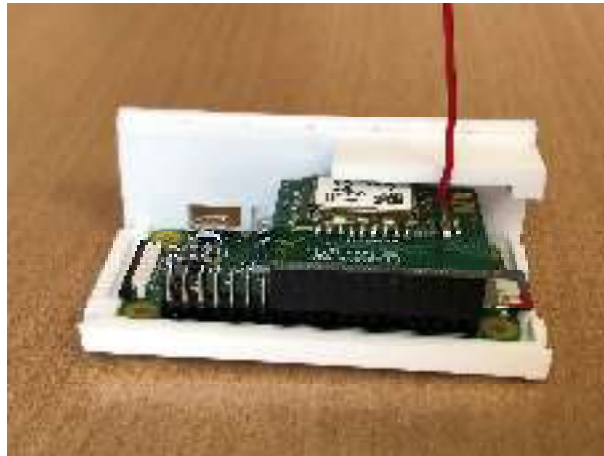


**Figure 57: EnOcean Repeater based on Raspberry Pi Zero and TCM310**

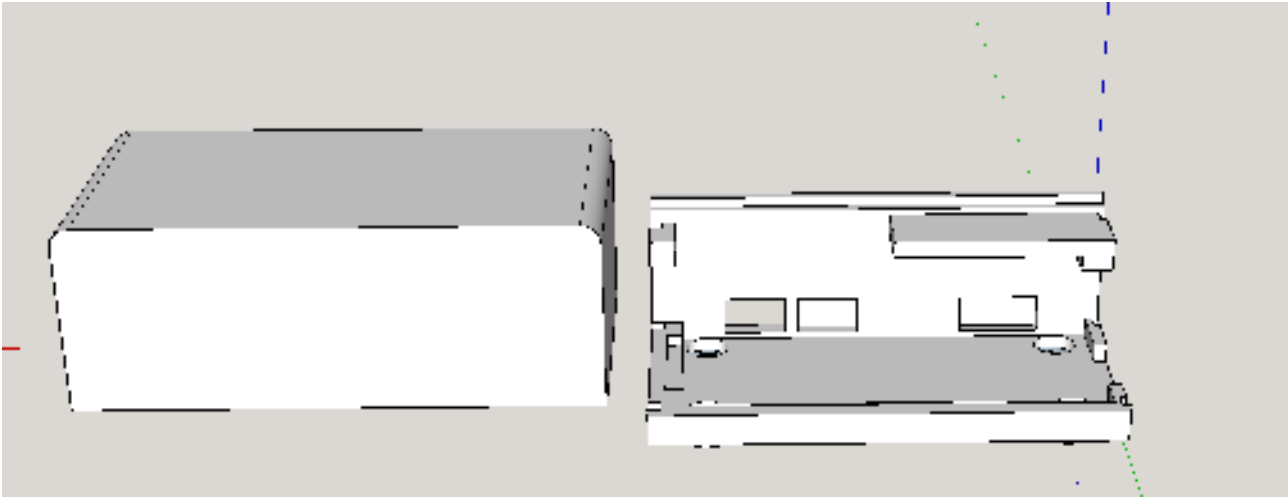


**Figure 58: 3D printed housing for the repeater**

Table 5 shows the component list required for the GREAT Repeater.

**Table 5: GREAT Repeater component list**

1	Raspberry Pi Zero W board
1	EnOcean Pi Module with TCM310
1	3D Printed Housing
1	Micro USB Power Supply, 1A
1	microSDHC card, 16GB, Class 10 (industrial)

## 6 Sensor Technology

### 6.1 Sensors for acquiring activation and relaxation status

The sensors used to detect changes in the activation and relaxation level of the group follow two approaches. Ambient PIR (passive infrared) sensors measure group activity based on frequency of motion detection. As soon as at least one person is in the room, the system uses the PIR sensors to continuously determine the relative activity level in the room (estimated number of entries/exits per time unit, estimated number of persons, total movement per area and person). The PIR data cannot be assigned to any person.

Body worn sensors are in use for caregivers to measure activity level and stress level. Wearables and smart textile for the patients are not in use due to the vulnerability of the target group and expected difficulties with acceptance and adherence.



### 6.1.1 PIR Sensor

The standard use case for PIR sensors is triggering lighting on basis of detected movement or presence. Part of further investigation is the detection of inactivity. Can the presence of inactive presence be recognized by history knowledge about the number of persons entered the room? For GREAT the main aspect is monitoring of activity and detection of group activity levels.

For the activation of lighting the sensor is typically triggered once by motion or presence and switches the light. For a period of 60-90 seconds or more the light is activated and the sensor falls into a sleep mode to conserve energy. After that sleep period the sensor starts to detect activity again. If no activity is detected, the light is switched off otherwise the light stays on and another sleep period starts.

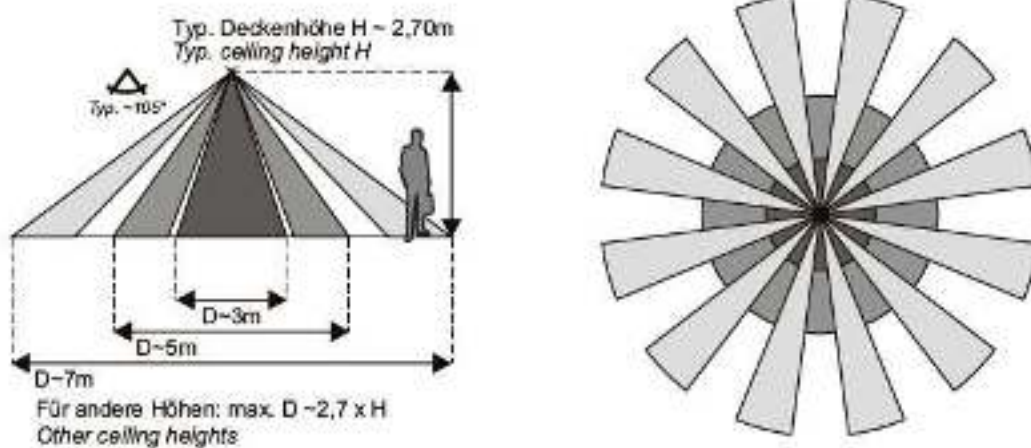


**Figure 59: Detection range**

The requirement for GREAT is to continuously detect activity. Therefore, the sleep period has to be as short as possible. To support convenient and modular installation the second requirement is wireless technology. Since there is a conflict between a wireless and energy-saving architecture and high frequency detection the chosen product has to be modified. The minimum sleep period was reduced to about 1 second. An additional modification is made due to the fact, that the sensor is placed on top of the ceiling and not as concealed installation (see Figure 60). If the human heat source moves through the individual zones, different charge differences are generated on the associated sensor elements and a movement can be detected over a large. The main issue would be to recognize not only movements and classify a single person's activities as shown in (Nef et al. 2015; Luo et al. 2017), but also how group activities can be classified and what this means related to a stressful or too calm situation. The sensor uses an optical shell combined with a magnetic cap to provide easy access in case of battery change without the necessity to completely removing the sensor. For GREAT the Thermokon "EasySens" SR-MDS BAT will be used (for technical specifications see Table 6, picture see Figure 60).

**Table 6: Technical specification for Thermokon SR-MDS BAT**

Vendor	Thermokon Sensortechnik GmbH (Germany)
Series	EasySense
Type	SR-MDS BAT
Retail price	250,00 EUR
Technical design	Wireless
Wireless technology	EnOcean ISO/IEC 14543-3-10
Radio frequency	868,3 MHz
Functions	Motion detection and brightness measurement
Motion detection	Passive infrared
Detection area	360°; 105° conical (ceiling installation)
Detection radius (2,5 m room height)	3,25 m
Power source	3 x Battery 3,6V 1/2 AA LS14250
Brightness (Accuracy)	0-510 Lux (+/- 30 Lux)
Sleep time interval (modified)	1s – 1000s



**Figure 60: Thermokon SR-MDS BAT with extra light 3D printed cover**

### 6.1.2 Body worn sensor

Changes in activity and stress or relaxation level can be measured by body worn sensors, which measure corresponding physiological parameters like heart rate, skin conductance or motion patterns via accelerometers. The Everion sensor from the company Biovotion (Zurich, Switzerland) makes use of various sensing techniques which can all be applied on the upper arm. There are several optical channels based on different colours to detect changes in subcutaneous tissue and a galvanic skin response sensor (GSR). Based on this raw data the human understandable vital parameters are calculated. The vitals available are listed in Table 7. The most interesting and most often used parameter for stress recognition is the heart rate variability (HRV). It is calculated based on the beat to beat (R-R interval) as illustrated in Figure 63. The HRV of a well-conditioned heart is typically large at rest. It might decrease in case of activity or interesting for us in case of mental stress. Biovotion applies to root mean squared of successive differences (RMSSD) to calculate the HRV. For our algorithm to recognize stress phases as shown in Figure 63, we apply three functions on the R-R intervals (according to Ulrich Reimer et al., 2017):

- SDNN: standard deviation of RR intervals (i.e., intervals between two heart beats)
- RMSSD: root mean square difference of successive RR intervals in the time frame
- PNN50: percentage of pairs of adjacent RR intervals differing by more than 50 ms.



**Figure 61: Biovotion Everion upper arm sensor**



**Figure 62: Everion back with light and galvanic skin sensors**

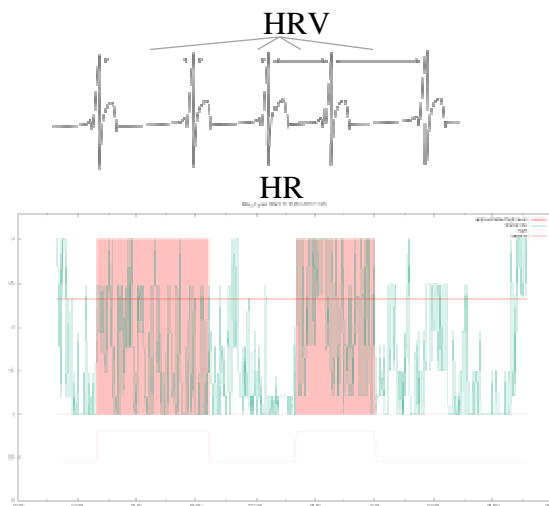


**Figure 63: HRV signal and marked high stress segments**

Therefore, we need the R-R values in milliseconds which are provided every second (1Hz). Together with the main vitals, a quality value in the range of 0-100 is provided. Values with a quality below 50 are ignored.

The algorithm applied in detail to derive the stress segments with the result shown in Figure 63 is described in detail in (Ulrich Reimer et al. 2017).

Another interesting testing parameter for our application might be the GSR, also referred to as Electrodermal Activity (EDA), which measures changes when starting to sweat. This is commonly used as a sensitive measure for emotional arousal. The GSR provided every second is expressed in a value between 0 – 65535 and has a conversion factor of 1/3000.

The advantage of the Everion in comparison to other sensors is its approval in Europe as a medical device for heart rate (HR) and blood oxygenation or oxygen saturation (SpO<sub>2</sub>) and its ISO certifications (ISO 1345). An approval by the FDA in the USA is currently ongoing. Also, the higher level of acceptance is an advantage which has been shown in

our tests at the sleep laboratory where the device has been applied by over 40 healthy test persons and over 30 unhealthy persons in parallel to ECG with electrodes attached and wrist worn devices (Reimer et al. 2017). The sensor is lightweight and convenient to wear, can store data locally, transmit data in real-time or whenever in range of a gateway and can be recharged easily by placing the sensor onto a conductive charging cradle. The comfortable wearing is supported by an elastic textile band available in different sizes as shown in Figure 64.



**Figure 64: Different sizes of bands for an optimal fit**

**Table 7: Technical specification for Biovotion Everion**

Vendor	Biovotion AG (Switzerland)
Type	Everion
Price (project)	550,00 EUR
Technical design	Wireless with rechargeable battery
Wireless technology	Bluetooth 4.0 + LE (IEEE 802.15.1)
Transmission range	<10 m
Radio frequency	2,4 GHz
Parameters	Heart rate Blood oxygenation Skin temperature Skin blood perfusion Steps / Motion



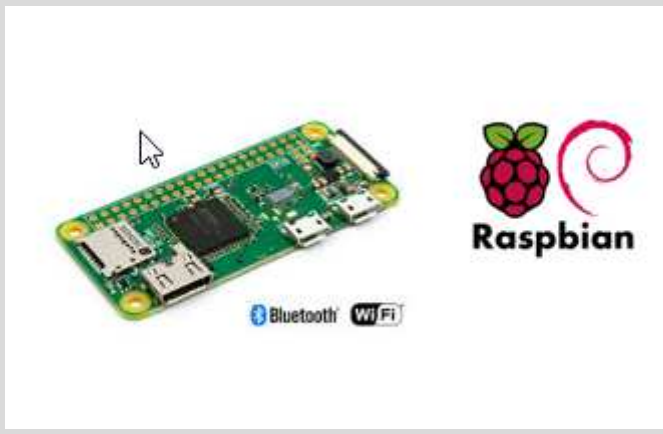
Experimental parameters (project)	Respiratory rate Heart rate variability Energy expenditure Blood pulse wave Skin conductance
Data modes	Vital sign parameters, raw data, mixed mode
Battery life	24 h
Power source	Embedded Li-Ion battery rechargeable

The sensor can transmit pre-calculated vital sign data or raw data from every parameter channel in real-time or buffer it to the internal memory. The memory can hold several days of vital sign data or 4 hours of raw data. The sampling rate of raw data at 53 Hz with 12 different channels causes a heavy data volume which leads to asynchronous data transmission over time (transmission is slower than recording of raw data).

In GREAT the vital sign mode is the preferred mode since the basic vital parameters are calculated in real-time for detection of changes in activation/relaxation and physical activity levels. For receiving data, a gateway has to be installed. Different variations are currently evaluated and considered for use. The preferred gateway is a Raspberry Pi 3 board controller which is also in use as the main controller of the GREAT system. Alternatives can be smartphones with an Android operating system or a Raspberry Pi Zero, which is the cheapest of all variations. The vendor currently only supports Windows and Android operating systems. Those variations rely on more expensive hardware like Stick-PCs based on Intel architecture, which is in conflict with a cheap end user price. To provide maximum compatibility and avoid problems with different Bluetooth stacks of different hardware components the vendor developed his own BT-Dongle. This dongle is also expensive (120 CHF). Different alternatives including advantages and disadvantages as well as the price tag are listed below (Figure 65).

For the functional tests, we started with the PC-Stick version and transfer the collected vitals every evening to our Cloud Server where also the logs from all devices are stored.

Originally, for the field tests, we planned for the cheaper variant with a Raspberry Pi 3 running Android. However, while porting the software, unexpected driver issues occurred. Therefore, we kept the working solution from the functional tests for the field test prototypes.

Variation	Pro/Cons	Price (CHF)
Intel Stick-PC with Windows 10 and BT-Stick		
	<p>Pro: Use of existing software</p> <p>Cons: Expensive Stability issues</p>	250
Raspberry Pi 3 with Windows		
	<p>Pro: Cheap</p> <p>Cons: Porting of software</p>	170
Raspberry Pi Zero with onboard BT		
	<p>Pro: Cheap Board in use in other modules</p> <p>Cons: Porting of software</p>	30


Raspberry Pi 3 with Android		
	<p>Pro:</p> <ul style="list-style-type: none"> <li>Cheap</li> <li>Software under development by vendor</li> </ul> <p>Cons:</p> <ul style="list-style-type: none"> <li>Stability issues</li> </ul>	60
Raspberry Pi 3 with Wine Emulation		

Figure 65: Possible hardware combinations incl. price tags

## 6.2 Environmental Sensor

In order to get more information about the environment where the GREAT system is being used and integrated, environmental sensor unit (BOSCH BME 680) has been incorporated into the scent module using a ready-made breakout board for easier placement and connection (see Figure 66).

The environmental sensor unit is connected to the controller of the Scent module via an I2C interface. It allows for measurements of air quality (VOC - Volatile Organic Compounds), temperature, pressure and relative humidity (see Table 8).



Figure 66: Watterott Bosch BME 680 breakout board



**Table 8: Bosch BME 680 Environmental Units Specification**

Interface	I <sup>2</sup> C and SPI
<b>Gas sensor</b>	
Response time ( $\tau$ 33-63%)	< 1 s (for new sensors) +/- 15% +/- 15
Sensor-to-sensor deviation	< 0.1 mA in ultra-low power mode direct output of IAQ: Index for Air Quality
Power consumption	
Output data processing	
<b>Humidity sensor</b>	
Response time ( $\tau$ 0-63%)	8 s
Accuracy tolerance	$\pm 3$ % relative humidity
Hysteresis	$\leq 1.5$ % relative humidity
<b>Pressure sensor</b>	
RMS Noise	0.12 Pa (equiv. to 1.7 cm)
Sensitivity Error	$\pm 0.25$ % (equiv. to 1 m at 400 m height change)
Temperature coefficient offset	$\pm 1.3$ Pa/K (equiv. to $\pm 10.9$ cm at 1°C temperature change)

## 7 Controller

The main controller is based on a Raspberry Pi 3 single board-computer (Figure 67). It features a Broadcom BCM2837 system on a chip with four ARM Cortex-A53 cores clocked at 1.2 GHz. It includes 1 GB of LPDDR2 RAM and features a 10/100 Ethernet port, a 2.4 GHz 802.11n wireless module and a Bluetooth 4.1 LE module. For extension, it offers 4 USB2 ports and a 40-pin GPIO header (e.g. providing support for I2C, I2S, SPI, UART interfaces).

To integrate EnOcean components, a Raspberry Pi EnOcean module based on the TCM310 EnOcean transceiver module is connected to the built in UART via the GPIO header of the Raspberry. For better signal performance of the EnOcean modules, an external 868 MHz antenna was originally connected to the EnOcean module, however, tests during the field trials have shown that the integrated antenna of the EnOcean module would be sufficient, if it's straightened. Table 9 lists the hardware components required for the GREAT controller.

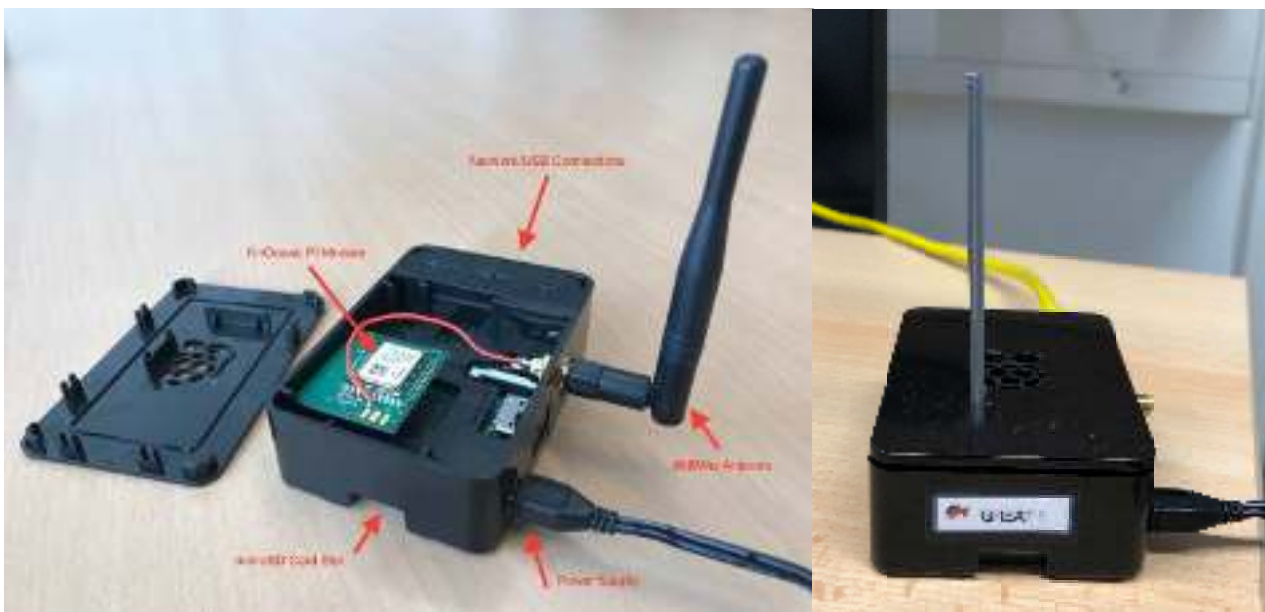


**Figure 67: Controller setup based on Raspberry Pi 3 and EnOcean PI 868 MHz module with external antenna on the left, and wire-antenna on the right.**

**Table 9: GREAT Controller hardware component list**

1	Raspberry Pi 3 board
1	Casing for Raspberry Pi 3
1	Micro USB Power Supply, 2.5A
1	microSDHC card, 16GB, Class 10 (industrial)
1	EnOcean PI 868 module for Raspberry
1	868MHz Antenna H-Tronic 1618110
1	SMA-Connector Socket

The reasons for choosing the Raspberry Pi 3 board as basis for the controller instead of other single board computers (e.g. like the Beagle Bone boards) were price, strong community support including a wide range of extensions, and most importantly built-in wireless support.

For a documentation of the software architecture and features of the field test prototype see Deliverable 2.4.

## 8 References

- [1] Lighting concept based on literature search see D1.1
- [2] Carvalho, DZ., St Louis, EK., Knopman, DS., Boeve, BF., Lowe, VJ., Roberts, RO., Mielke, MM., Przybelski, SA., Machulda, MM., Petersen, RC., Jack, CR., Vemuri, P. (2018) Association of excessive daytime sleepiness with longitudinal  $\beta$ -Amyloid Accumulation in Elderly Persons Without Dementia. *JAMA Neurol.* 75(6): 672-680.
- [3] Shokri-Kojori. E., Wang, GJ., Wiers, CE., Demiral, SB., Guo, M., Kim, SW., Lindgren, E., Ramirez, V., Zehra, A., Freeman, C., Miller, G., Manza, P., Srivastava, T., De Santi, S., Tomasi, D., Benveniste. H., Volkow, ND. (2018)  $\beta$ -Amyloid accumulation in the human brain after one night of sleep deprivation. *Proc Natl Acad Sci USA* 115(17): 4483-4488. doi: 10.1073/pnas.1721694115.
- [4] Ulrich Reimer; Emanuele Laurenzi; Edith Maier; Tom Ulmer (2017): Mobile Stress Recognition and Relaxation Support with SmartCoping: User-Adaptive Interpretation of Physiological Stress Parameters Hilton Waikoloa Village, Hawaii, USA, January 4-7, 2017. In: 50th Hawaii International Conference on System Sciences, HICSS 2017, Hilton Waikoloa Village, Hawaii, USA, January 4-7, 2017: AIS Electronic Library (AISeL). Online verfügbar unter [http://aisel.aisnet.org/hicss-50/hc/apps\\_for\\_health\\_management/5](http://aisel.aisnet.org/hicss-50/hc/apps_for_health_management/5).
- [5] Reimer, Ulrich; Emmenegger, Sandro; Maier, Edith; Zhang, Zhongxing; Khatami, Ramin (2017): Recognizing Sleep Stages with Wearable Sensors in Everyday Settings. In: Proceedings of the 3rd International Conference on Information and Communication Technologies for Ageing Well and e-Health. 3rd International Conference on Information and Communication Technologies for Ageing Well and e-Health. Porto, Portugal: SCITEPRESS - Science and Technology Publications, S. 172–179.

## 9 List of figures

Figure 1: GREAT Components Overview, Source: GREAT consortium.....	6
Figure 2: Schematic representation of the lighting solution in GREAT. The biodynamic curve is running automatically, light interventions (activation, relaxation, TV scene) are adjustable manually or automatically.....	8
Figure 3: Biodynamic lighting concept. CCT...colour temperature in Kelvin, Eh...horizontal illuminances of the task light, $E_{h_{Room}}$ ...horizontal illuminance of ambient room light (resulting from $E_v + E_h$ Task, for clarity reasons $E_{h_{Room}}$ is not shown), $E_v$ ...vertical illuminance at the eye level.....	9
Figure 4: GREAT lighting concept.....	9
Figure 5: Activating light cue.....	10
Figure 6: Relaxing light cue.....	11
Figure 7: Different control options for the GREAT luminaire: basic functions (left), advanced functions (right).....	11
Figure 8: Increasing the vertical illuminance by adding a diffuse panel to the luminaire (left) and reaching high horizontal illuminances by adding task lighting by spots (right)....	12
Figure 9: Results of light pressure study.....	13
Figure 10: Optical concept for the GREAT Uplight (left) and the 2 possible Luminous Intensity Distribution curves LID (right): The Indirect light is available as an asymmetric solution for the wall mounted luminaire and as a symmetrical light distribution for example for the free-standing luminaire situated in the middle of the room.....	14
Figure 11: Picture of the Uplight of the GREAT luminaire.....	14
Figure 12: The LEDs are placed on the edge for lateral input of light in the light guiding plate.....	15
Figure 13: Dialux simulation of the GREAT Uplight.....	15
Figure 14: Downlight of the GREAT luminaire and LPG.....	16
Figure 15: Dialux simulation of the GREAT Uplight and Downlight.....	16
Figure 16: Spot of the GREAT luminaire.....	17
Figure 17: Dialux simulation of the GREAT Uplight, Downlight and Spot.....	17
Figure 18: Dialux simulation of the GREAT Uplight, Downlight and Spot, results The values listed in the table are already achieved with warm white LEDs (2200K). With cold white LEDs (5000K) higher illuminances can be achieved.....	18
Figure 19: Technical specification sheet GREAT luminaire.....	19
Figure 20: Dialux simulation of the GREAT luminaire showing the illuminances in a 25 m <sup>2</sup> room. ....	20

Figure 21: Dialux simulation of the light distribution of the GREAT luminaire. Also shown are the isolines for 150 lx (orange), 300 lx (yellow) and 600 lx (grey) horizontal illuminance. ....20

Figure 22: Dialux simulation of the GREAT luminaire showing the luminances in a 25 m<sup>2</sup> room. ....21

Figure 23: Free-standing, mobile GREAT luminaire..... 21

Figure 24: Wall-mounted GREAT luminaire in a patient's room in the hospital in Hall (Austria) ..... 22

Figure 25 : The buckling mechanism of the free-standing luminaire..... 22

Figure 26: Special adjustment for psychiatric institutions: breaking point for protection against suicide..... 23

Figure 27: GREAT system implemented in a patient's room in the hospital in Hall (Austria) .24

Figure 28: GREAT standing luminaire in the common area in the hospital in Hall (Austria)..24

Figure 29: New, optimized luminaire head with EnOcean board and driving board .....25

Figure 30: EnOcean switch ..... 26

Figure 31: EMV measurement of the GREAT luminaire for CE conformity..... 26

Figure 32: Transportable GREAT Luminaire ..... 27

Figure 33: Easy adjustment of GREAT luminaire ..... 28

Figure 34: Cable storage feature ..... 28

Figure 35: GREAT sound module based on Logitech Z150 active speaker ..... 29

Figure 36: Raspberry PI and Pi-DAC Zero integrated into the Z150 active speaker.....30

Figure 37: 3D model of Raspberry PI + Pi-DAC Zero holder for mounting inside Z150 speaker .....31

Figure 38: Wiring of the Pi-DAC 2x4 header to the Logitech board inside the speaker ..... 31

Figure 39: 3D model of separate housing for sound module logics..... 32

Figure 40: External sound module with a Pioneer RM05 Speaker featuring a frequency range of 40-50.000Hz..... 33

Figure 41: Speaker covers to prevent accidental adjustment of volume level .....33

Figure 42: Sine, linearization and database for linearization and formula for the linear approximation ..... 35

Figure 43: Error between sine and linear approximation, absolute [-1, 1] and percentage 35

Figure 44: Evolution of mount (top), piston (center left), eccentric (center right) and lever (bottom) ..... 36

Figure 45: Left shows the no-load-phase of the motor, right shows the spring-tensioning-phase of the motor..... 37

Figure 46: Reworked mechanic installed in the rear casing ..... 37

Figure 47: Evolution of the 3D-printed front casing (top) and the two variants of shields (bottom) .....	38
Figure 48: Left shows the completely mounted rear casing, right shows the front casing...	39
Figure 49: Microcontroller; left unprotected; right covered.....	40
Figure 50: Raspberry Pi Zero W board computer .....	40
Figure 51: Adafruit DRV8833 motor driver breakout board.....	41
Figure 52: Adafruit 12bit ADC converter ADS1015 breakout board.....	41
Figure 53: Current flow to motor during pump cycles with no bottle inserted (top), and bottle inserted bottom) as raw signal and smoothed signal. ....	42
Figure 54: Schematics for the electrical components of the scent module. ....	42
Figure 55: Printed circuit board design for the scent module electronics. ....	43
Figure 56: VOC sensor mounting .....	43
Figure 57: EnOcean Repeater based on Raspberry Pi Zero and TCM310 .....	45
Figure 58: 3D printed housing for the repeater .....	46
Figure 59: Detection range .....	47
Figure 60: Thermokon SR-MDS BAT with extra light 3D printed cover .....	49
Figure 61: Biovotion Everion upper arm sensor.....	50
Figure 62: Everion back with light and galvanic skin sensors .....	50
Figure 63: HRV signal and marked high stress segments .....	50
Figure 64: Different sizes of bands for an optimal fit .....	51
Figure 65: Possible hardware combinations incl. price tags .....	54
Figure 66: Watterott Bosch BME 680 breakout board.....	54
Figure 67: Controller setup based on Raspberry PI 3 and EnOcean PI 868 MHz module with external antenna on the left, and wire-antenna on the right. ....	56

## 10 List of tables

Table 1: Advantages and disadvantages of diffuse and task lighting .....	12
Table 2: GREAT Light Module hardware component list .....	28
Table 3: GREAT Sound Module hardware component list .....	32
Table 4: GREAT Scent Module hardware component list .....	44
Table 5: GREAT Repeater component list.....	46
Table 6: Technical specification for Thermokon SR-MDS BAT.....	48
Table 7: Technical specification for Biovotion Everion .....	51
Table 8: Bosch BME 680 Environmental Units Specification .....	55
Table 9: GREAT Controller hardware component list .....	57